Modeling of radiative divertor experiments with argon seeding for H-mode plasma in EAST

Zhongshi Yang[1,a)], Jingbo Chen[1], D. P. Coster[2], Yanmin Duan[1], Liang Wang[1], Fang Ding[1], Jichan Xu[1], Qing Zang[1], Tengfei Wang[1], Ning Yan[1], Tao Zhang[1], Ling Zhang[1], Jinhua Wu[1], Yueng-Kay Martin Peng[1], and Guang-Nan Luo[1]

[1]*Institute of Plasma Physics, Chinese Academy of Sciences, Hefei 230031, China*
[2]*Max Planck Institute for Plasma Physics, EURATOM Association, D-85748 Garching, Germany*

ABSTRACT

To obtain a quantitative understanding of recent radiative divertor experiments and to give an instructive prediction for future relative work performed on EAST, The 2D numerical tool SOLPS has been used to investigate the argon seeded EAST H-mode plasmas. The simulations were mainly based on a typical H-mode discharge with lower single null divertor configuration, in which the partially detached divertor plasma has been achieved due to the argon seeding. First the perpendicular particle and energy transport coefficients for particle density diffusivity $D_{\perp}$, electron and ion conduction, $\chi_{\perp i,e}$ were radially varied to determine the edge transport barrier in H-mode plasma by comparing the simulated upstream profiles of electron temperature (T_e) and electron density (n_e) with the edge Thomson scattering data. Then the reduction of the particle flux, static pressure and the peak heat load onto the lower outer divertor target have been reproduced by radiative divertor simulations in agreement with the experimental measurements, which demonstrated that the argon seeding is effective to mitigate the heat load onto the divertor target and achieve partially detached plasma during H-mode discharge. The simulations also revealed that the strongest radiation occurred near the X-point and in the divertor region for short pulsed argon seeding with a relatively low puffing rate in agreement with bolometer measurements.

[a)] *Corresponding author. Electronic mail: zsyang@ipp.ac.cn*

I. INTRODUCTION

The scientific missions of EAST are to explore the reactor relevant operation regimes with long pulse lengths and high plasma core confinement and to develop and verify solutions for power exhaust and particle control in steady operational state[1-3]. Mitigation of particle flow and heat flux from the high temperature core plasma deposited on the divertor surface is a key issue for magnetic confinement fusion device including EAST and future ITER when operated in long pulse, high power regime[4-6]. The primary solution to the above mentioned problem is to introduce inert gas impurities such as neon or nitrogen into divertor plasma, reduce the scrape-off layer heat flux and to cool the divertor plasma to detachement by radiation of the impurities. On the other hand, Impurity seeding will result in the sputtering of the divertor target materials. Therefore, the radiative dissipation must be achieved with acceptable consequences for the plasma performance in terms of confinement of core plasma, radiative cooling of divertor plasma, reduction of the impact energy of the sputtering particle and dilution of burning plasmas[7, 8].

EAST is presently equipped with fully actively cooled plasma facing components (PFCs), carbon tiles near the divertor strike points and molybdenum (Mo) tiles for main chamber wall, and has a capability of near 14MW heating power source, which enabled the achievement of a long-pulsed high confinement mode (H-mode) operation while brought out a great threat to safety of the divertor target due to excessive heat load. Since the extensive upgrade of EAST's internal PFCs, a series of radiative divertor experiments for L-mode and H-mode discharges in EAST have been carried out. By seeding the impurity gas (mainly argon (Ar) and mixture of Ar with D_2), the partially detached divertor plasma has been achieved, in which scenario the particle flux, plasma temperature and heat load onto the divertor target have been reduced dramatically. The experimental results will be described in section 2of this work.

To obtain a quantitative understanding of the physics processes in divertor detachment experiments, 2D numerical tools are often used by comparing the theoretical models to existing radiative divertor experiments. Furthermore, the modeling would help to give an instructive prediction for future relative work performed on exiting Tokamaks and future fusion devices. In ASDEX upgrade, SOLPS 5.0 (B2.5-EIRENE)[9] have been used extensively to study the H-mode divertor detachment with impurity seeding[10-13]; while in JET, H-mode plasmas in radiative divertor experiments were investigated[14,15] by using EDGE2D-EIRENE[16]. In EAST, SOLPS 5.2 (B2-EIRENE) and SOLPS 5.1 have also been used to understand the radiative divertor operation

towards detachment in typical L-mode discharge[17,18]. In this work, SOLPS 5.0 (B2.5-EIRENE) was used to study the radiative divertor experiments with Ar seeding for a typical H-mode discharge.

II. EXPERIMENT

The presented radiative divertor experiment with Ar seeding was performed in a typical H-mode discharge (#52353) with lower single null divertor configuration. The main parameters in this shot was as follows: plasma current Ip = 450 kA, toroidal field Bt = 2.5 T with the ▽B-drift pointing into the lower divertor, line averaged plasma density ne = $3.3\times10^{19}/m^3$, 1.7MW neutral beam heating and 2.2 MW ion cyclotron resonance heating in turn. After the NBI heating power was injected to the plasma at t = 2.8 s, the plasma density and the stored energy increased dramatically accordingly. The plasma entered a Type-I ELMy H-mode regime at t = 3.0 s following the fluctuations of D_a signals observed by spectroscopy. FIG. 1 shows the time evolution of the main plasma parameters during discharge #52353. The particle balance was maintained by the gas puffing near the inner midplane and pumping. During the shot time t = 3.2-3.4 s, the Ar mixture with D_2 (1:4) was seeded from near the separatrix strike point at the outer target plate with a seeding rate of 1.1 $pa.m^3/s$ (namely total particle flux of 2.5×10^{20} /s with Ar flux of 0.5×10^{20}/s). At the shot time t = 3.275 s, the plasma parameters n_e, V_{loop} and stored energy started to respond to the Ar seeding , which means the delay time was around 100 ms due to the limitation of pipe length for the seeding inlets during the radiative divertor experiments. The total radiation power P_{tot} measured by AXUV (absolute extreme ultraviolet) bolometer arrays increased with shot time during the Ar seeding since t = 3.275 s and reached a maximum value of 0.8 MW at t = 3.4 s, which was about the 50% total heating power. It brought a great loss of stored energy due to the increase of P_{tot}, and the heat load deposited onto the target was decrease dramatically. From the measurements of infrared camera, the surface temperature near the separatrix strike point at the outer divertor target during the H-mode phase decreased from 100℃ before Ar seeding to 50℃ after Ar seeding with a relatively flat surface temperate distribution profile along the outer divertor target, which indicated that the Ar seeding has significant effect on the mitigation of peak heat flux to the target. At the same time, Ion saturation current (J_{sat}) at the inner and outer divertor target started to response to the Ar seeding at shot time t = 3.3 s and decreased by 50% at least near the strike point with time during the Ar

seeding (FIG. 2.), showing that the divertor plasma started to partially detach on the outer target during the inter-ELM phases, and the ELM size decreased considerably.

III. MODELING

A. Simulations of EAST H-mode plasma during inter-ELM phase

In this session, simulations of the presented radiative divertor experiments with Ar seeding for H-mode plasma in EAST was performed by SOLPS code package[9], which consists of two coupled codes: the fluid plasma code B2.5 deal with the the Braginski-like equations for the ions and electrons. EIRENE the Monte-Carlo code describes kinetic neutrals. Both codes are coupled via source terms. The primary purpose of running the simulations was to reproduce the reduction of power deposition and particle flux onto the divertor target and also to depict the radiation distribution with increasing Ar seeding. The cross-field transport coefficients for electron and ion conduction, $\chi_{\perp i,e}$, particle density diffusivity $D_{\perp}$, control the rate of perpendicular particle and energy diffusion. $D_{\perp}$ and $\chi_{\perp i,e}$ are free parameters in SOLPS modeling, which usually are set as constants in real space in L-mode simulations. H-mode plasma are associated to the formation of an internal transport barrier occurred in the vicinity of LCFS with greatly reduced transport and steep radial gradients from SOL to plasma core region [19]. In SOLPS, it is possible to vary the transport coefficients in radial direction in three regions: one is on closed field lines, the second is the steep H-mode pedestal close to the separatrix and the third is outer SOL region with larger radial plasma transport coefficients [9]. At high temperatures (midplane, near separatrix), corrections for flux limit are necessary due to the fact that the heat conduction mean free path is larger than the connection length. The flux limit is defined as

$$q_{lim}=\alpha_{e,i} n_{e,i} T_{e,i}^{3/2} m_{e,i}^{1/2}.$$

The values of heat flux limiters adopted in this work were $\alpha_{e,i}=0.3$ and $\alpha_{,i}=1.0$.

The first step was to model the steady state, inter-ELM period of none-impurity seeded H-mode plasmas. In this work, the ELM dynamics has been precluded. The upstream density and temperature are important experimental plasma parameters in SOLPS modeling, which are used to find appropriate transport coefficients. However, during the radiative divertor experiments the experimental density and temperature profile in the upstream SOL region were not available. Therefore, a typical lower single null (LSN) H-mode discharge #48914 was selected for the SOLPS modeling. In this shot, the upstream temperature and density data were given by

measurements of Edge Thomson Scattering (TS). The magnetic configuration and the SOLPS numerical grids for this shot is shown in FIG. 3. The main plasma parameters for this shot were: line averaged density $3\times10^{19}/m^3$, heating power 3.7 MW including neutral beam heating, lower hybrid wave heating and Ohmic heating, plasma current 450 KA, toroidal field 2.3 T with the ∇B-drift pointing into the lower divertor.

For a given heating power P, it is assumed that 20% of the heating power is radiated as bremsstrahlung and cyclotron radiation from the core plasma according to the analysis of the power balance in the SOL plasma[17,20], so P_{solps} = 80% P is assumed for the present modelling. For the simulations of discharge #48914, P_{solps} was assumed to be 3.0 MW. no exact experimental data are available since a separation of P_e and P_i is not possible in the experimental measurement, therefore, 1.5 MW of P_e and 1.5 MW of P_i are assumed in this simulation. Separatrix density ne_{sep} feedback was used throughout the simulations. The gas puff was described inside the EIRENE input file as a point source of D_2, placed on the vessel midplane from where it was introduced to the simulated grids as in experiments.

Three groups of vessel surfaces were adopted: the first was tungsten for upper divertor, the second was molybdenum for chamber wall and the third was carbon for lower divertor. Physical sputtering was implemented accordincg to the standard Roth-Bodansky model and chemical sputtering yield from D^+ and D impact was set to constant as Y_{ch} = 0.03 on the carbon surfaces. Both physical and chemical ion sputtering occurred at the carbon divertor targets and no ion sputtering was assumed at tungsten and molybdenum surfaces. Thus the simulated fluids in B2.5 included neutrals of deuterium and carbon, ion species of D^+ and all charge states of carbon. No drifts have been included in the simulations presented in this work.

Coefficients, $D_\perp$, $\chi_{\perp i,e}$ were systematically radially adjusted (FIG. 4) until the satisfactory agreement between experimental and simulated midplane profiles were obtained by comparing the results for upstream profiles of T_e, Ti and n_e with the Edge Thomson Scattering data (FIG. 5). The TS profiles compiled of a number of pulses through the discharge, filtered to exclude ELM events. The diffusion coefficient $D_\perp$ ranged from 0.05 $m^2.s^{-1}$ in the core region, 0.1 $m^2.s^{-1}$ near the separatrix. While for the $\chi_{\perp i,e}$, the values were adopted from just inside the inner boundary of the simulation region right through the edge transport barrier ranged from 7.8 $m^2.s^{-1}$ to 3.0 $m^2.s^{-1}$. In the main SOL, both $D_\perp$ and $\chi_\perp$ were increased up to a value of 1.0 $m^2.s^{-1}$ and 10.0 $m^2.s^{-1}$

respectively. A higher value of $D_\perp$ and $\chi_\perp$ in the main SOL were applied in order to flatten the temperature profiles there. Through the above radial profiles variations of the transport barrier of particle and heat diffusivities, a steep pedestal region inside the magnetic separatrix has been reproduced.

After the midplane profiles were matched, the transport coefficients in the divertor region were varied until the outer target profile peak values were fitted to the experimental measurements by divertor LP. The radially constant heat conductivities (2.0 $m^2.s^{-1}$) and particle diffusivities (0.4 $m^2.s^{-1}$) in the divertor plasma below the X-point were adopted in the simulations. The LP data were chosen from different time slices around simulated time slice at shot time t = 5.06 s at the inter-ELM phase. Here the ion saturation current (J_{sat}) and electron temperature (T_e) from the LP measurements at the lower outer target and lower inner target were taken to compared with SOLPS modeling results. J_{sat} is not an output of simulations, so the j_{sat} was calculated from the particle flux and the angel between the magnetic flux line and the target. FIG. 6 presents the measured lower outer and inner divertor target J_{sat}, T_e profiles compared with the simulations. For the outer divertor target, the simulation results for the j_{sat} agreed well with LP data near the strike point and slightly underestimated the LP datat within a factor of 1 away from the strike point. While for the electron temperature, SOLPS still could give the peak value measured from LP near strike points but with larger underestimation in the region away from the strike point. For the inner divertor target, the simulation results for the j_{sat} also agreed well with LP data near the strike point but underestimated the LP data from the strike point. While for the electron temperature, SOLPS gave higher peak value than the measured data from LP near strike point but with slightly underestimation in the region away from the strike point. It was found experimentally that the J_{sat} for lower outer divertor target was lower than the J_{sat} for lower inner target while the T_e for lower outer target was higher than the T_e for lower inner target. This inboard/outboard asymmetry of the experiment was also reproduced by the simulations as shown in FIG. 6.

B. Simulations of EAST radiative divertor experiments with Ar seeding

Once the steady state H-mode discharge without impurity seeding was reproduced by SOLPS, the transport parameters in the upstream and divertor region were used for the modeling of the

radiative divertor experiments with Ar seeding. The simulations were mainly based on discharge #52353 described in section 2. In this discharge, Ar gas was injected into the divertor plasma from the outer divertor target from 3.2 s to 3.4 s. Before the Ar seeding simulation, a steady state inter-ELM H-mode was still needed to be simulated as starting point for initial conditions subjected to the succeeding modeling. For this simulation, the magnetic equilibrium configuration and plasma parameters in time slice of shot time t = 3.2 s were adopted. Ar was injected into the computational domain from near the strike point at the lower outer divertor target with a puffing rate of 5×10^{19} particles/s.

FIG. 7 shows the simulated outer divertor target profiles of particle flux and static pressure before and after Ar seeding, which have been compared with experimental results from LP measurements. Simulated particle flux and electron temperature were taken from the simulated time t = 0 s and t = 100 ms separately indicating a simulated seeding duration of 100ms, while the experimental data from LP measurements were taken from shot time t = 3.2 s and t = 3.4 s respectively indicating a seeding duration of 200 ms. The reason we chose different time for comparison was that there was a delay for the Ar gas to enter the divertor region and response to the divertor plasma since the gas valve has been opened as mentioned in section 2. Before Ar seeding as shown in FIG. 7, the simulated pressure and particle flux were in good agreement with the experimental data. The peak particle flux has been decreased from $7\times10^{23}/m^2.s$ to $3\times10^{23}/m^2.s$ while the static pressure decreased from 300 Pa to 80 Pa, which was still in a good agreement with LP data. The loss of pressure and particle flux has been reproduced by simulations indicating the formation of partially detached divertor plasma due to the Ar seeding. The power flux deposited onto the target was the divertor parameter we most concerned about. From the simulation results, it was shown that the peak heat flux was decreased from 1.6 MW/m^2 to 200 kW/m^2, demonstrating that the Ar seeding was effective to mitigate the heat load onto the divertor target and achieve partially detached plasma during H-mode discharge.

Two AXUV cameras, each with 32 channels, installed in EAST at the same toroidal location, were designed to fully cover the poloidal cross-section of plasma. The viewing chords distribution of the AXUV arrays are shown in FIG. 8(a). The AXUV measurements were compared to reconstructed line integrated power densities from the simulations in FIG. 8(b). Agreement was attained in the divertor region and top SOL region. In the region close to the X-point, the modeled radiation power density was higher than experimental measurements by a

factor of 2. Within the rage between channel 10 and channel 55 covering the core region, AXUV measurements were systematically higher than the simulations, for the core radiation in the simulated line integrals was not taken into account. For the Ar seeding with a relatively low puffing rate (5×10^{19} particles/s) and short pulsed puffing duration (100 ms) according to the simulations, the strongest radiation occurred near the X-point and in the divertor region while there was still a significant portion of radiated power dissipated within the core boundary region. The total radiated power in this simulation was 1.02 MW while the total radiated power was 0.93 MW from bolometer measurements which covered the main plasma region and partial inner divertor region. Considering the domain size deviation between the simulation which did not cover partial core region and the experiment which did not cover partial divertor region, there was good agreement for the total radiation between simulation and experiment. The Z_{eff} was 3.20 in the simulation for the simulated region while the experimental value was 2.72 for the main plasma region. This difference could also be mainly attributed to the different computed domain between the simulation and the experiment. Contributions for the radiation losses from tungsten and molybdenum were not included in this simulation. In EAST only upper divertor is tungsten with fully actively cooling and the lower target is still carbon materials, with molybdenum used for main chamber wall. In this work, the simulated discharge (#52353) had a lower single null divertor configuration. For this scenario, the sputtering from the upper divertor and main chamber wall was comparably negligible and the argon dominated the impurity radiation in the edge plasma region as well as the main plasma region. This was confirmed by the edge impurity spectrum for the divertor region and EUV (extreme ultraviolet spectrometer) diagnostics for the core plasma region.

VI. CONCLUSIONS

To mitigate the heat load deposited onto the divertor target during the EAST H-mode discharge, radiative divertor experiments with Ar seeding have been performed in a typical H-mode discharge with lower single null divertor configuration. The partially detached divertor plasma has been achieved, with the dramatic increase of the total radiation power and significant reduction of the ion saturation current and the target surface temperature.

SOLPS code package was used to simulate the above mentioned radiative experiment. The first step was to model the steady state, inter-ELM period of none impurity-seeded H-mode

plasmas for the purpose of defining the perpendicular particle and energy transport coefficients for particle density diffusivity $D_{\perp}$, electron and ion conduction $\chi_{\perp i,e}$. Coefficients $D_{\perp}$, $\chi_{\perp i,e}$ for the upstream plasma were systematically radially varied until the satisfactory agreement between experimental and simulated midplane profiles were obtained by comparing the results for upstream profiles of T_e and n_e with the edge Thomson Scattering profiles. The coefficients in the divertor region below X-point was kept as constant to achieve an agreement for the peak value of ion saturation current and electron temperature between simulations and experiments from LP measurements.

The simulations of radiative divertor experiments with Ar seeding for EAST H-mode discharge have reproduced the reduction of the particle flux, static pressure and the peak heat load onto the lower outer divertor target, which was in agreement with the experimental measurements, demonstrating that the Ar seeding was effective to mitigate the heat load onto the divertor target and achieve partially detached plasma during H-mode discharge. To analyze the radiation distribution, the AXUV measurements were compared to reconstructed line integrated power densities from the simulations which revealed that the strongest radiation occurred near the X-point and in the divertor region for short pulsed Ar seeding with a relatively low puffing rate.

According to the analysis of simulations, the radiation power fraction, radiation distribution and the moving speed of radiation front towards core region were sensitive to puffing rate and duration time. Excessive Ar puffing would lead to the accumulation of Ar particles in the core region thus the strong core radiation, even the disruption of discharge. Therefore, besides the validation between experiments and simulations, the predictive modeling on future EAST radiative divertor experiments is very important for the study of radiative divertor in EAST and will have great significance for the next-step experiments by choosing appropriate seeding rate and duration, as well as different seeding impurity.

ACKNOWLEDGMENTS

This work is partially supported by National Magnetic Confinement Fusion Science Program of China under Contract Nos. 2013GB105002 and 2013GB105001, National Natural Science

Foundation of China under Contract Nos.11575242 and 11305214. The authors would like to thank the EAST team for the experimental data.

REFERENCES

[1]J. Li, H. Y. Guo, B. N. Wan, X. Z. Gong, Y. F. Liang, G. S. Xu, K. F. Gan, J. S. Hu, H. Q. Wang, L. Wang, L. Zeng, Y. P. Zhao, P. Denner, G. L. Jackson, A. Loarte, R. Maingi, J. E. Menard, M. Rack and X. L. Zou, *Nature Physic*s **9**, 817–821 (2013).

[2]B. Wan , J. Li, H. Guo, Y. Liang, G. Xu, X. Gong, EAST Team and International Collaborators, *Nucl. Fusion* **253**, 104006 (2013).

[3]H. Y. Guo, J. Li, B. N. Wan, X. Z. Gong, Y. F. Liang, G. S. Xu, X. D. Zhang, S. Y. Ding, K. F. Gan, J. S. Hu, L. Q. Hu,S. C. Liu, J. P. Qian, Y. W. Sun, H. Q. Wang, L. Wang, T. Y. Xia, B. J. Xiao, L. Zeng, Y. P. Zhao, P. Denner, J. R. Ferron, A. M. Garofalo, C. T. Holcomb, A. W. Hyatt, G. L. Jackson, A. Loarte, R. Maingi, J. E. Menard, M. Rack, W. M. Solomon, X. Q. Xu, M. Van Zeeland, X. L. Zou and EAST Team, *Phys. Plasmas* **21**, 056107 (2014).

[4]M. Shimada, D.J. Campbell, V. Mukhovatov, M. Fujiwara, N. Kirneva, K. Lackner, M. Nagami, V.D. Pustovitov, N. Uckan and J. Wesley, *Nucl. Fusion* **47**, S1–S17 (2007).

[5]C.S. Pitcher, P.C. Stangeby, *Plasma Phys. Control. Fusion* **39**, 779 (1997).

[6] A. Loarte, B. Lipschultz, A.S. Kukushkin, G.F. Matthews, P.C. Stangeby, N. Asakura, G.F. Counsell, G. Federici, A. Kallenbach, K. Krieger, et al., N*ucl. Fusion* **47**, S203–S263 (2007).

[7]A. Kallenbach, M. Bernert, R. Dux, L Casali, T Eich, L Giannone, A Herrmann, R McDermott, A Mlynek, H W Müller, et. al., *Plasma Phys. Control. Fusion* **55**, 124041 (2013).

[8]G.J van Rooij, J.W Coenen, L. Aho-Mantila, S. Brezinsek, M. Clever, R. Dux, M. Groth, K. Krieger, S. Marsen, G.F Matthews, A. Meigs, R. Neu, S. Potzel, T. Putterich, J. Rapp, M.F Stamp, *J. Nucl. Mater.* **438**, S42-S47 (2013).

[9]R. Schneider X. Bonnin, K. Borrass, D.P. Coster, H. Kastelewicz, D. Reiter, V. A. Rozhansky, B. J. Braams, Contrib. *Plasma Phys.* **46**, 3 (2006).

[10]M. Wischmeier, M. Groth , A. Kallenbach, A.V. Chankin, D.P. Coster, R. Dux, A. Herrmann, H.W. Müller, R. Pugno, D. Reiter, A. Scarabosio, J.G. Watkins, DIII-D team and ASDEX Upgrade team, *J. Nucl. Mater.* **390–391**, 250–254 (2009).

[11]L. Aho-Mantila, M. Bernert, J. W. Coenen, R. Fischer, M. Lehnen, C. Lowry, S. Marsen, K. McCormick, H. W. Müller, B. Sieglin, M. F. Stamp, M. Wischmeier, X. Bonnin, D. P. Coster, D. Reiter, S. Brezinsek, ASDEX Upgrade Team, JET-EFDA Contributors, *J. Nucl. Mater.* **438** (Suppl.), S321–S325 (2013).

[12]F. Reimold, M. Wischmeier, M. Bernert, S. Potzel, A. Kallenbach, H.W. Müller, B. Sieglin, U. Stroth andthe ASDEX Upgrade Team, *Nucl. Fusion* **55,** 033004 (2015).

[13]F. Reimold, M. Wischmeier, M. Bernert, S. Potzel, D. Coster, X. Bonnin, D. Reiter, G. Meisl, A. Kallenbach, L. Aho-Mantila, U. Stroth, the ASDEX Upgrade Team, *J. Nucl. Mater.* **463** 128-134 (2015).

[14]A. E. Jaervinen, M. Groth, M. Airila, P. Belo, M. Beurskens, S. Brezinsek, M. Clever, G. Corrigan, S. Devaux, P. Drewelow, et . al., *J. Nucl. Mater.* **463**, 135-142 (2015).

[15]A.E. Jaervinen, C. Giroud, M. Groth, P. Belo, S. Brezinsek, M. Beurskens, G. Corrigan, S. Devaux, P. Drewelow, D. Harting, et . al., *Nucl. Fusion* **56**, 046012 (2015).

[16]S. Wiesen, EDGE2D/EIRENE code interface report, JET ITC-Report, 2006, see http://www.eirene.de/e2deir_report_30jun06.pdf.

[17]Y. Chen, F. Q. Wang, X. J. Zha, L. Q. Hu, H. Y. Guo, Z. W. Wu, X. D. Zhang, B. N. Wan, and J. G. Li, *Phys. Plasmas* **20**, 022311 (2013).

[18]H. Du, C. Sang, L. Wang, X. Bonnin, H. Guo, J. Sun, D. Wang, *Plasma Phys. Control. Fusion* **58**, 085006 (2016)

[19]J. Wesson, Tokamaks, (Clerendon Press, Oxford, 2004), Chap. 4.

[20]D. N. Hill, B. Braams, J. Haines, J. Milovich, T. Rognlien, D. P. Stotler, and M. Ulrickson, *Fusion Technol.* **21**, 1263–1264 (1992).

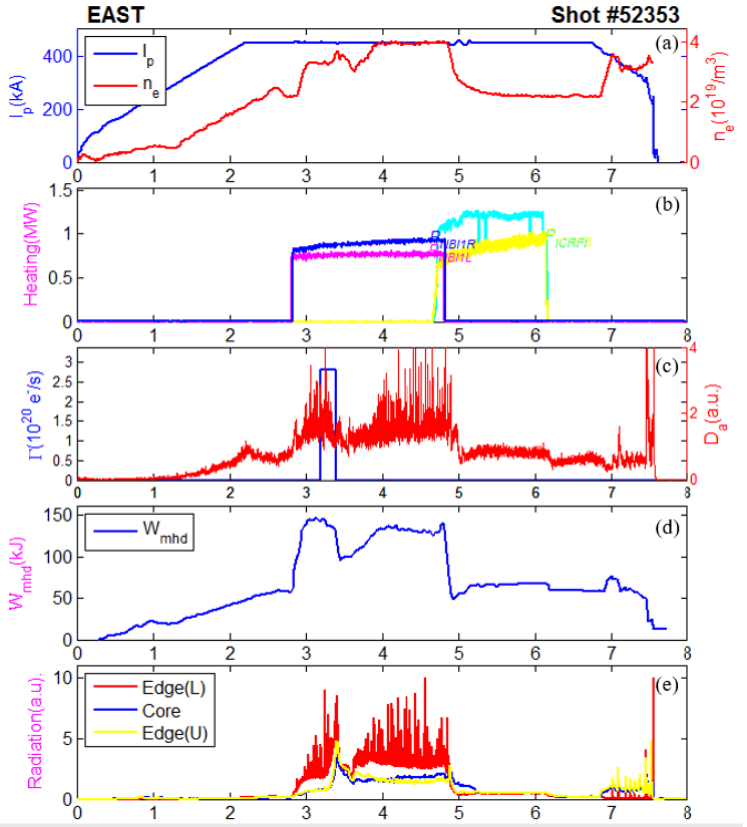

FIG. 1. Time evolution of the main plasma parameters during discharge #52353: (a) plasma current and line averaged electron density; (b) heating power: P_{NBI} and P_{ICRF}; (c) mixture (Ar: D_2) seeding rate and D_a spectrum intensity in lower divertor region; (d) stored energy (W_{MHD}); (e) radiation in core, upper and lower region.

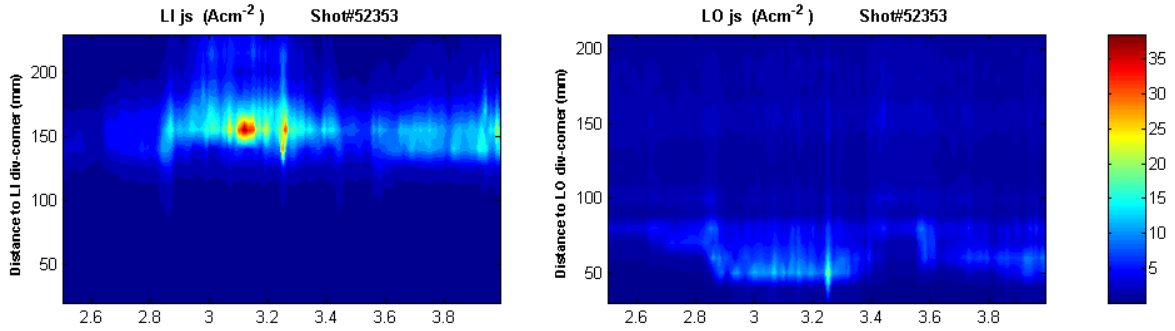

FIG. 2. Time evolution of ion saturation current density (j_s) at lower inner target (LI) and lower outer target (LO).

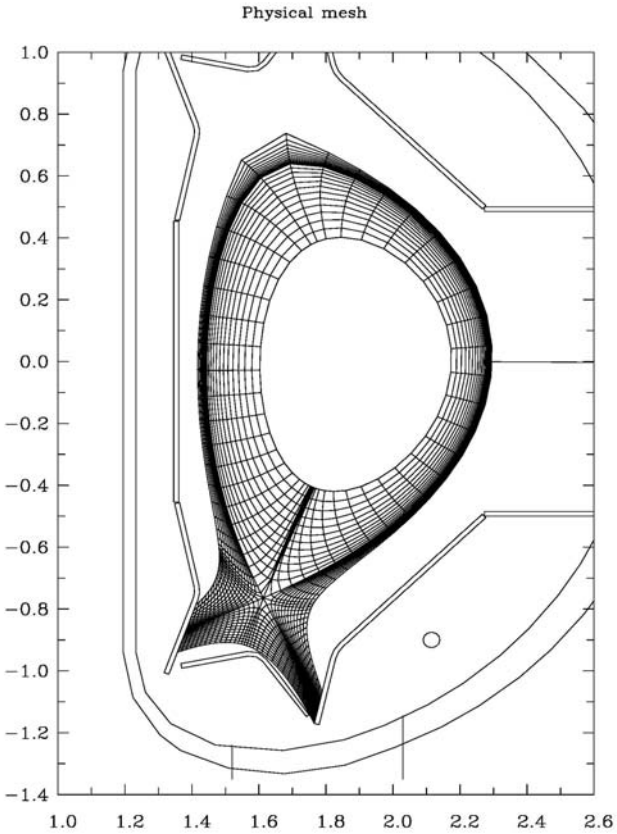

FIG. 3. The magnetic configuration and the SOLPS numerical grids for discharge #48914.

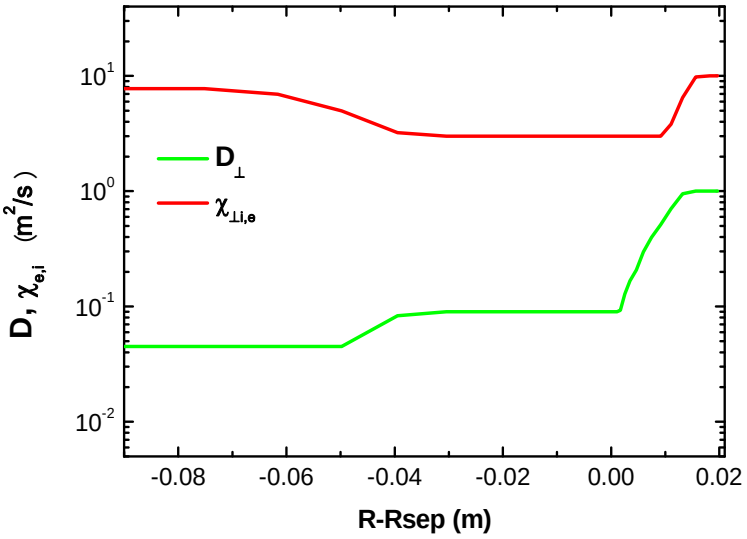

FIG. 4. The cross-field transport coefficients for electron and ion heat conduction ($\chi_{\perp i,e}$) and for particle diffusion ($D_\perp$).

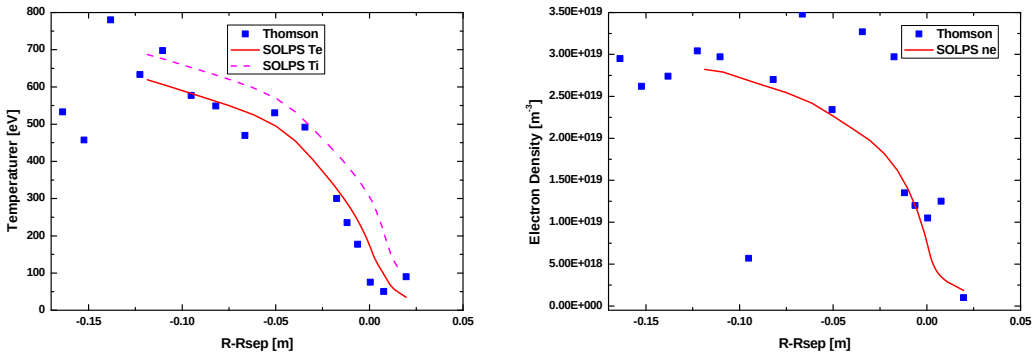

FIG. 5. The midplane electron temperature (solid line), ion temperatures (dashed line) and electron density calculated from SOLPS compared with experimental data measured from Edge Thomson Scattering for discharge #48914.

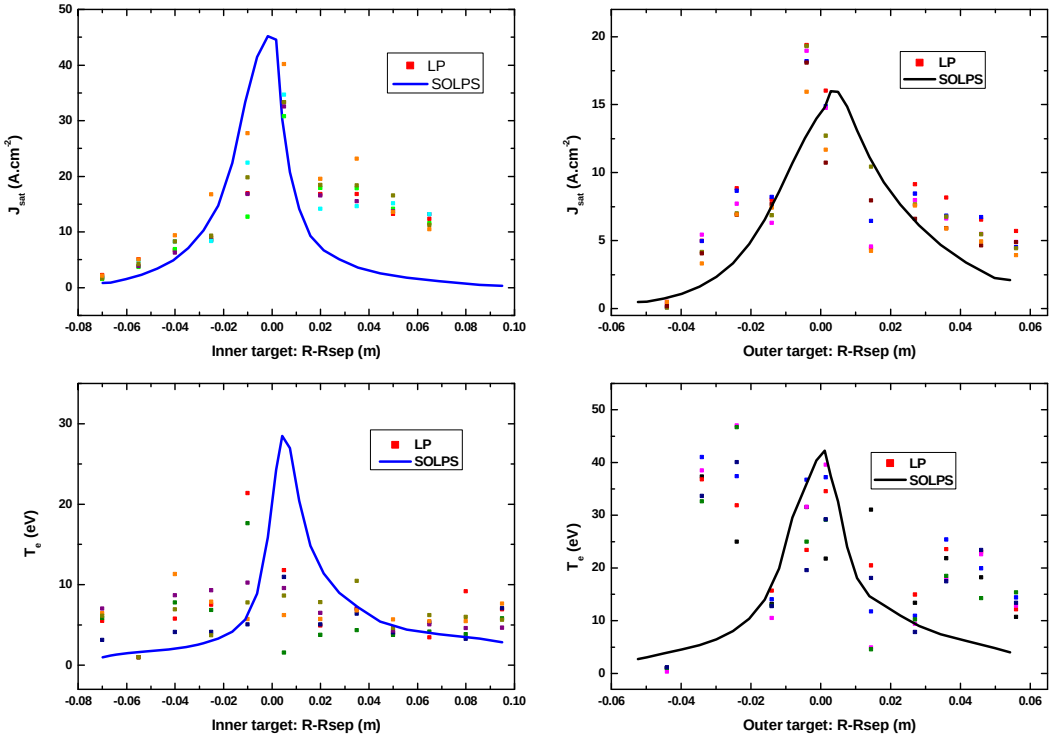

FIG. 6. The ion saturation current density and electron temperature at lower inner target (left) and lower outer target (right) calculated from SOLPS compared to experimental data measured from Langmuir Probe for discharge #48914.

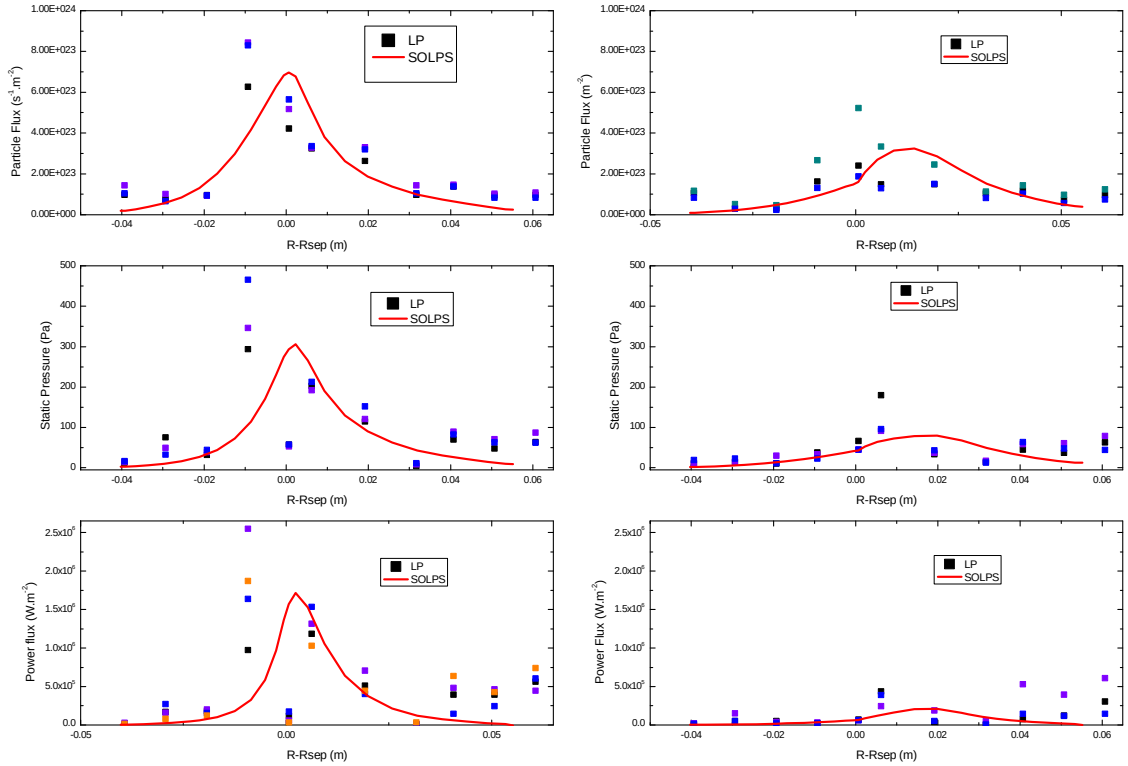

FIG. 7. The particle flux, static pressure, and power flux at lower outer target calculated from SOLPS compared to experimental data measured from Langmuir Probe for discharge #52353 before (left) and after (right) Ar seeding.

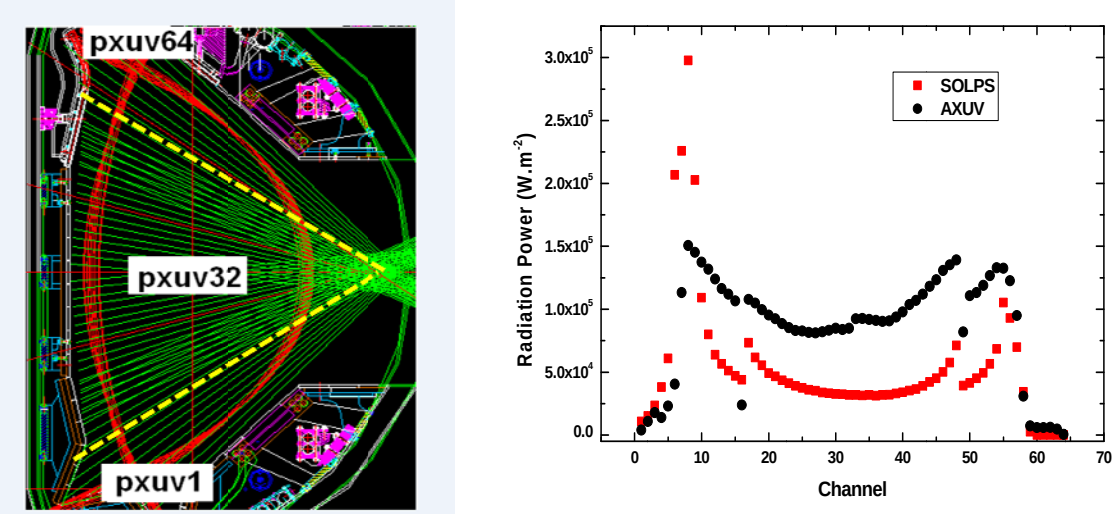

FIG. 8. The viewing chords distribution of the AXUV (left) and the AXUV measurements compared to reconstructed line integrated power densities from the SOLPS simulations for Ar seeded discharge #52353 (right).